

Microstructural characterization of polycrystalline materials by synchrotron X-rays

Leyun WANG (✉)¹, Meimei LI¹, Jonathan ALMER², Thomas BIELER³, and Rozaliya BARABASH⁴

¹ Nuclear Engineering Division, Argonne National Laboratory, Lemont, IL 60439, USA

² X-ray Science Division, Argonne National Laboratory, Lemont, IL 60439, USA

³ Department of Chemical Engineering & Materials Science, Michigan State University, East Lansing, MI 48824, USA

⁴ Materials Science & Technology Division, Oak Ridge National Laboratory, Oak Ridge, TN 37831, USA

© Higher Education Press and Springer-Verlag Berlin Heidelberg 2013

ABSTRACT: Third generation synchrotron X-rays provide an unprecedented opportunity for microstructural characterization of many engineering materials as well as natural materials. This article demonstrates the usage of three techniques for the study of structural materials: differential-aperture X-ray microscopy (DAXM), three-dimensional X-ray diffraction (3DXRD), and simultaneous wide angle/small angle X-ray scattering (WAXS/SAXS). DAXM is able to measure the 3D grain structure in polycrystalline materials with high spatial and angular resolution. In a deformed material, streaked diffraction peaks can be used to analyze local dislocation content in individual grains. Compared to DAXM, 3DXRD is able to map grains in bulk materials more quickly at the expense of spatial resolution. It is very useful for studying evolving microstructures when the materials are under deformation. WAXS/SAXS is suitable for studying materials with inhomogeneous structure, such as precipitate strengthened alloys. Structural information revealed by WAXS and SAXS can be combined for a deeper insight into material behavior. Future development and applications of these three techniques will also be discussed.

KEYWORDS: differential-aperture X-ray microscopy (DAXM); three-dimensional X-ray diffraction (3DXRD); wide angle/small angle X-ray scattering (WAXS/SAXS)

Contents

- 1 Introduction
 - 2 Differential-aperture X-ray microscopy
 - 3 Three-dimensional X-ray diffraction
 - 4 Wide angle/small angle X-ray scattering
 - 5 Summary and outlook
- Abbreviations
Acknowledgements
References

Received February 25, 2013; accepted March 28, 2013

E-mail: leyunwang@anl.gov

1 Introduction

Hard polycrystalline materials such as metals and ceramics are by far the most widely used group of structural materials in today's manufacturing industry. Performance of these materials is to a large extent governed by their microstructure and its evolution under deformation. For example, the well-known Hall–Petch equation describes an inverse relationship between the yield strength of a polycrystalline metal and its grain size as $\sigma_y = \sigma_0 + kd^{-1/2}$, where σ_0 is a friction stress, k is a material constant, and d is the average grain diameter [1]. The Hall–Petch relationship is often interpreted using the dislocation

theory: with a smaller grain size, the mean glide distance and pile-up length for dislocations in a single grain generally decreases, which requires a higher external stress for them to transmit through the grain boundary and eventually cause macroscopic yielding of the material [2–3]. In addition to the grain size, the distribution of grain orientations (i.e. texture) also affects the plasticity of a polycrystalline material, as the activation of slip or twinning systems in a grain usually follows the Schmid law [4].

Today, the dominant set of tools for characterizing microstructure in polycrystalline materials is electron microscopy (EM). Owing to its high spatial resolution (< 1 nm), transmission electron microscopy (TEM) continues to be an indispensable tool for studies of dislocations, interfaces, and precipitates in metallic materials [5]. However, the investigation area by TEM is sometimes too small to ensure that the observed effects are representative of the whole material. Scanning electron microscopy (SEM), on the other hand, offers a larger investigation area than TEM, but its spatial resolution is usually lower than TEM [6]. In the last two decades, SEM imaging in combination with automated electron backscattering diffraction (EBSD) has been effectively used to characterize grain structure and micro-plasticity effects in polycrystalline metals [7–10]. Prior to deformation, grain geometry and grain orientation from a large surface area of the material can be quickly measured and presented in a statistical way (e.g. grain size distribution, pole figure, etc.). After deformation, slip bands and deformation twins observed in individual grains can be quantitatively analyzed for a physics-based understanding of plasticity and material failure mechanisms [11–13].

Despite the versatility of EM, it has a universal and critical limitation: the low penetration depth of electrons (< 0.1 μm for most metals), which means only the surface region can be probed. However, the most important microstructural features (e.g. grain boundaries, dislocation substructure, twins, cracks, etc.), are often three-dimensional (3D) in nature. By only observing a two-dimensional

(2D) section of the material, the opportunity to fully understand many processes such as twin nucleation from a grain boundary or crack initiation from a subsurface inclusion cannot be observed or analyzed. Furthermore, grains on the surface are essentially in a different environment from the majority of the grains in the bulk material because the free surface imposes less constraint on the surface grains. This implies that findings made from surface observation may not be applicable to the material in the interior. While 3D morphology, crystallography and chemistry maps can be achieved by performing serial sectioning [14–16], the sample is totally destroyed after the characterization so that further investigation becomes impossible. In addition, sectioning may introduce strain relaxation and/or microstructural changes at the newly-created surfaces making true ‘bulk’ characterization impossible.

Hard X-rays generated from synchrotron radiation is an ideal way to non-destructively characterize the 3D microstructure of a bulk material. High speed electrons produced by particle accelerators ($\sim 99.999\%$ of the speed of light) are further accelerated by a booster synchrotron to $\sim 99.99999\%$ of the speed of light before being forced to travel in a closed circle (often called “storage ring”) by strong magnetic fields. At particular exit locations from the ring, specialized insertion devices (undulators and wigglers) allow constructive interaction between the magnetic fields and the high speed electrons to generate synchrotron X-rays with high flux, high brilliance (i.e. small source size), and a tunable energy range up to 300 keV [17]. Today, there are a growing number of sites where high quality synchrotron X-rays are generated at third-generation synchrotron light sources [18], such as those in Table 1. Because of their high penetration ability, third-generation synchrotron X-rays are an ideal probe for the study of bulk material microstructures.

In the last two decades, various techniques have been developed using synchrotron X-rays to characterize materials, including scattering, tomography, imaging, fluorescence and absorption spectroscopy. In this article,

Table 1 List of worldwide third-generation synchrotron light sources

Facility name	Location	Ring energy /GeV	Perimeter /m	Year commissioned
ESRF	France	6	844	1992
APS	USA	7	1060	1995
SPring-8	Japan	8	1436	1997
SLS	Switzerland	2.4	240	2001
SSRF	China	3.5	396	2007
PETRA-III	Germany	6	2304	2009

three scattering-related techniques very useful for metal-lurgy research are considered: differential-aperture X-ray microscopy (DAXM), three-dimensional X-ray diffraction (3DXRD), and wide angle/small angle X-ray scattering (WAXS/SAXS). DAXM and 3DXRD are two non-destructive techniques that allow individual grains in bulk polycrystalline materials to be studied. On the other hand, WAXS/SAXS is powerful for characterizing materials with a heterogeneous microstructure (e.g. second-phase precipitates, voids, etc.). For each technique, the working principles will be briefly summarized and their use will be demonstrated with a few application examples either from the literature or from the authors' work. The outlook of future research will also be discussed.

2 Differential-aperture X-ray microscopy

Differential-aperture X-ray microscopy (DAXM) is a technique developed by Oak Ridge National Laboratory and first installed at beamline 34-ID at Advanced Photon Source (APS) in USA [19]. A polychromatic X-ray microbeam with an energy range of 8–25 keV was obtained by focusing the X-rays using a pair of Kirkpatrick-Baez (KB) mirrors. The dimension of this microbeam is about $0.5 \mu\text{m} \times 0.5 \mu\text{m}$ at beamline 34-ID. It can penetrate the specimen (usually mounted at a 45° angle from the beam direction) on the order of 100 micrometers, depending on the electron density of the material. Laue diffraction peaks from all volumes along the beam path are generated and recorded on a CCD camera detector above the specimen. A moving Pt wire (diameter = $50 \mu\text{m}$) serves as the “differential aperture” to partially block diffracted X-rays, which enables Laue patterns from individual volume elements (voxels) to be reconstructed [20–22]. A schematic illustration of the DAXM method is shown in Fig. 1.

For an undeformed material, the reconstructed Laue patterns are usually characterized by sharp diffraction spots. These Laue patterns can be automatically indexed to determine the crystallographic orientation of its corresponding voxel. By moving the specimen along a line, or an array of lines, a 2D or 3D subsurface grain map can be obtained. Figure 2 shows an example where a 2D subsurface grain map in a commercial purity Ti specimen was measured by DAXM [23].

In a deformed sample, the presence of dislocations leads to both lattice curvature and lattice stretch. Therefore, in reciprocal space, diffraction can happen along directions that are near, but do not strictly satisfy the Bragg condition.

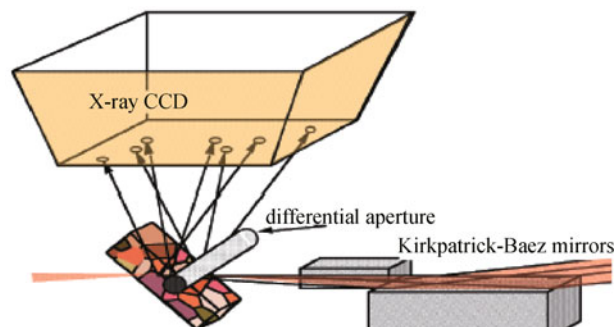


Fig. 1 A schematic illustration of the DAXM method. The X-ray microbeam is focused by a pair of KB mirrors and directed to the specimen. Laue diffraction patterns from individual voxels along the beam path can be extracted by using a differential aperture. (Reproduced with permission from Ref. [21], Copyright 2004 Springer)

As a result, Laue patterns often display broadened peaks. The shape of broadened peaks depends on the local dislocation content. Larson et al. [24] demonstrated that the absolute dislocation density tensor can be directly calculated by measuring individual components of the lattice curvature tensor and the strain tensor using DAXM. Barabash and Ice et al. took a different approach [20,25–26]. They noticed that in most cases, peak broadening is asymmetrical: the peak has an elongated direction ξ and a narrow direction ν . ξ and ν are perpendicular to each other, and both of them are perpendicular to the reciprocal vector \mathbf{g} of the diffraction plane. They found that the peak width in the narrow direction depends on the total dislocation density, while the peak width in the elongated direction only depends on the unpaired dislocations (geometrically necessary dislocations, GNDs). From the detailed analysis of inverse scattering problem, they proposed that a set of edge GNDs having Burgers vector \mathbf{b} , slip plane normal \mathbf{n} , and line direction $\boldsymbol{\tau} = \mathbf{b} \times \mathbf{n}$, will cause reflection (hkl) to elongate in the direction $\boldsymbol{\xi} = \frac{\boldsymbol{\tau} \times \mathbf{g}_{hkl}}{|\boldsymbol{\tau} \times \mathbf{g}_{hkl}|}$. From the observed peak streak direction, the slip system of the GNDs can be inferred. This method has been successfully used to identify GNDs in different materials [23,25–30].

After plastic deformation, polycrystalline metals often show slip traces on the surface. It is important to distinguish GNDs from dislocation activity characterized by surface slip traces [11,31–33]. These slip traces represent the intersection line between the active slip plane in the grain and the specimen surface. If the crystallographic orientation of the grain is known from diffraction information, then the orientation of all possible slip planes in this grain and the direction of the resultant

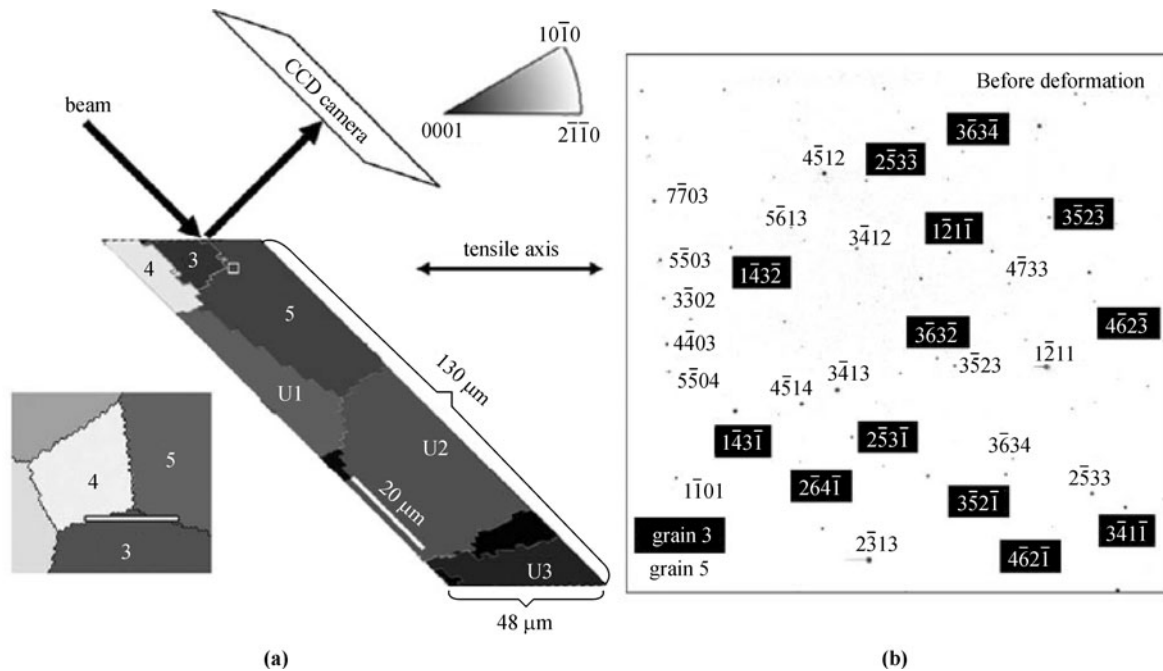


Fig. 2 Result from a DAXM line scan near the triple junction of three surface grains in a commercial purity Ti specimen. (a) A subsurface grain map was obtained by indexing Laue patterns for each voxel. (b) An exemplary Laue pattern from the white box next to the 3–5 grain boundary in (a). Peaks from both grains are indexed with indices from Grain 5 appearing in black text and indices from Grain 3 as white text in black boxes. (Reproduced with permission from Ref. [23], Copyright 2010 The Minerals, Metals & Materials Society and ASM International)

slip trace can be calculated. By comparing them with actual slip traces, one can identify the activated slip system(s). While this type of slip trace analysis is convenient for analyzing dislocation activity in a large number of grains, it is limited by the fact that slip traces only represent near-surface dislocation activity. Dislocations from deeper regions cannot be detected by this method. Furthermore, slip trace analysis may not be possible if the specimen shows little or no slip traces at all.

Figure 3 shows an example from a recent study of Ti–5Al–2.5Sn (wt.%) alloy deformed in a creep test. After about 13% engineering strain, most of the grains on the surface did not display slip traces, as shown in the SEM micrograph in Fig. 3. The lack of a slip trace, however, does not mean the absence of dislocation activity within the grain. A DAXM line scan across Grain C3 showed an apparent peak streak, which indicated an abundance of GNDs underneath the surface. Depending on the location, the peak streak direction was different in Grain C3. At the bottom of Fig. 3, Laue patterns from locations a, b, and c represent the streaked peaks in the orange, gold, and red regions of the map. By performing the peak streak analysis described above, the most likely type of GNDs was inferred for each region. In patterns a and b, the streak directions correspond to edge dislocations on one of the highly stressed $\langle c+a \rangle$ slip systems. The streak directions

in pattern c are close to those expected from a highly stressed prismatic slip system. It should be mentioned that this analysis, like most examples in the literature, attributes the observed peak streak (i.e. lattice rotation) to edge type GNDs. Even though GNDs identified by peak streak analysis were found to be consistent with nearby surface slip traces in several cases [23,28–30], one cannot rule out the possible existence of screw GNDs. To date, there is not an established prediction of peak streak and shape resulting from screw type GNDs [34–35].

Perhaps the best way to characterize the full dislocation structure in a grain is to combine DAXM and TEM. The general distribution of GNDs is first characterized by DAXM. Then, TEM specimens from selected regions can be made by focused ion beam (FIB) techniques [36] for analyzing localized dislocations. This way, GNDs identified by peak streak analysis can also be verified. However, such experiments may have difficulties from expected FIB-induced damage [37], or dislocation rearrangement due to the free surface that could alter the dislocation content in the specimen.

As a concluding remark, DAXM is able to map 3D grain structure in a polycrystal with high spatial and angular resolution. If analyzed properly, such 3D grain maps can be directly compared with crystal plasticity finite element modeling (CPFEM) [38–41]. Computational results from

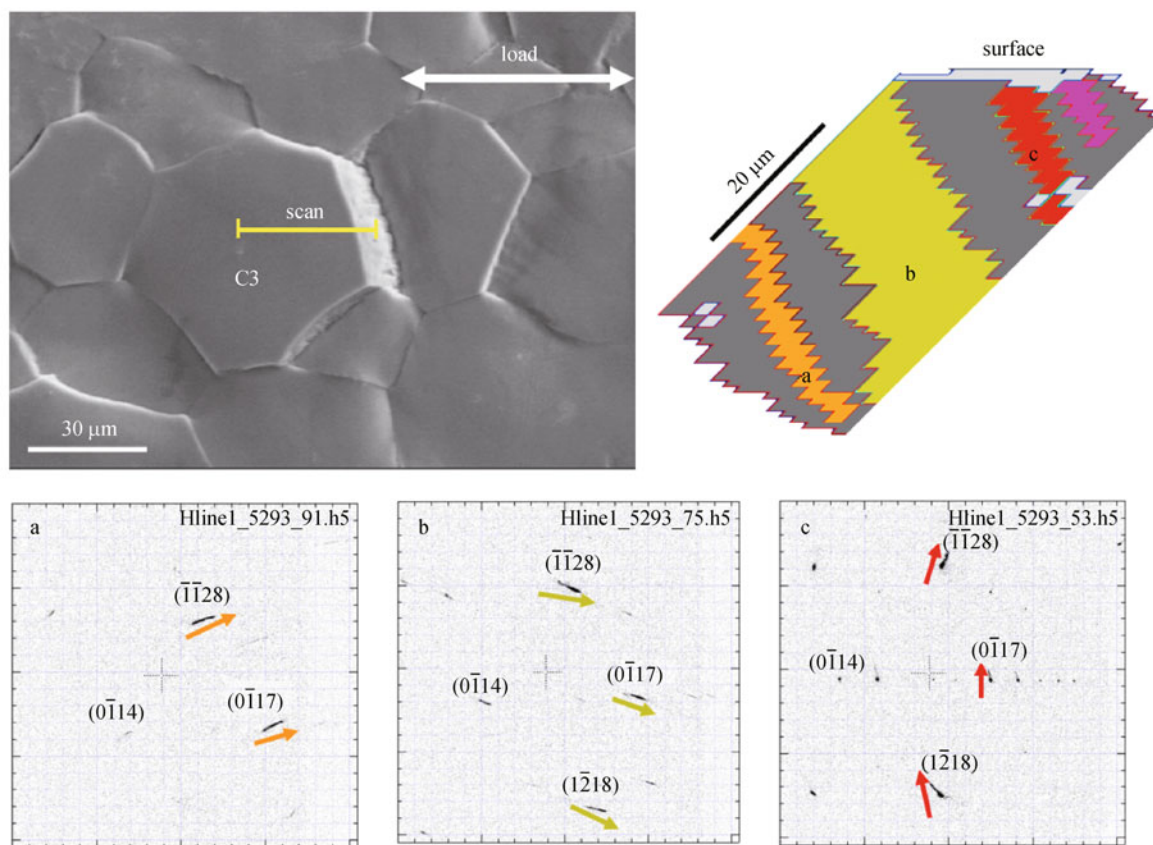


Fig. 3 A DAXM line scan was performed on a Ti–5Al–2.5Sn specimen after creep deformation to an engineering strain of ~13% at 728 K. The peak streak directions found inside Grain C3, which did not display surface slip traces, are illustrated in diffraction patterns. The subsurface map of Grain C3 is partitioned by color according to the appearance of Laue patterns: the orange, gold, red, and pink regions show peak streak in different directions. The dark grey region shows broadened peaks with complex shapes, while the light grey region shows sharp diffraction spots. Laue patterns from three voxels labeled a–c are shown. Peak streak analysis was performed to identify the GNDs in the orange, gold and red regions by a method described in Ref. [23].

CPFEM using true 3D grain structure (e.g. stress–strain curve, slip/twinning activity, lattice rotation, etc.) can be directly compared with experimental measurements to assess the quality of constitutive models. DAXM is also useful for probing GNDs underneath the surface, over grain-scale volumes which are important for understanding micro-plasticity but difficult to fully characterize by SEM or TEM.

Like all other techniques, DAXM has its limitation. First, the data acquisition speed is slow due to the differential aperture setup. Second, the penetration depth usually does not exceed 200 μm due to the X-ray energy that is typically used (8–25 keV). (Unfortunately, X-rays with higher energy is not suitable for DAXM because the differential aperture then needs to be much bigger in order to provide sufficient absorption, but this would deteriorate the spatial resolution.) Given that, DAXM is more useful for materials with a small grain size if one wants to obtain a 3D grain map in a reasonable amount of time to include

enough grains that can be considered as “grains in the bulk”. This limitation of DAXM can be overcome using 3DXRD, which will be discussed next.

3 Three-dimensional X-ray diffraction

Three-dimensional X-ray diffraction (3DXRD) was first developed at Risø National Laboratory in Denmark with a dedicated beamline ID11 at European Synchrotron Radiation Facility (ESRF) [42–46]. A similar beamline (1-ID) was built at APS later under an alternative name of high energy diffraction microscopy (HEDM) [47]. In this technique, a monochromatic X-ray beam with energy between 50–100 keV is used. The beam dimension is defined by a slit, which is usually narrow in the vertical direction (1–300 μm) and wide in the transverse direction (~1 mm). Unlike DAXM that adopts a “scanning” approach, 3DXRD uses a “tomographic” strategy. As shown in Fig. 4, the specimen is mounted on a ω rotation

stage. Illuminated by the incoming X-ray, any part of the specimen that satisfies the Bragg condition will generate a diffraction peak. Diffracted X-rays are recorded by one or more 2D detectors behind the specimen. To generate more diffraction events, the specimen is rotated around the z direction (i.e. vertical direction) with a step size of $\Delta\omega$ (typically $\Delta\omega = 1^\circ$). At each step, an exposure is made and a corresponding diffraction pattern is recorded on the 2D detectors. When the specimen finishes its rotation, all the diffraction patterns that were taken at different ω angles are combined to solve for the microstructure in the layer that was illuminated by the beam. Dedicated codes for peak searching and grain indexing are used. This scheme is similar to traditional tomography mapping.

Two types of detectors are typically used for different purposes. Near-field detectors with pixel size of $1\text{--}5\ \mu\text{m}$ are usually placed close to the specimen (detector distance $L = 2\text{--}20\ \text{mm}$); far-field detectors with pixel size of $50\text{--}200\ \mu\text{m}$ are usually placed further from the specimen ($L = 100\text{--}1000\ \text{mm}$) [48]. On the near-field detector, diffraction spots are distributed almost randomly. Because the detector distance is comparable to the specimen dimension, the position of a diffraction spot depends not only on the crystallographic orientation of the associated grain, but also on the spatial location of that grain. Solving the patterns

from the near-field detector allows the 3D grain structure to be reconstructed with a spatial resolution of $\sim 2\ \mu\text{m}$, and crystallographic orientation resolution of $\sim 0.1^\circ$ [49–51]. This technique is very useful for studying grain substructure evolution while the material is under heat treatment or deformation. In one study, Schmidt et al. [50] demonstrated 3D grain growth in an Al–0.1%Mn material under annealing, as shown in Fig. 5. In another study, Li et al. [51] showed the development of an intragranular orientation gradient induced by plastic deformation in a Cu wire.

On the far-field detector, diffraction spots form typical Debye–Scherrer rings. In this case, less spatial information can be extracted from the diffraction patterns (only the grain center position can be estimated), but the high angular resolution allows accurate stress characterization in individual grains. The algorithm is summarized as follows [52–56]: for a single grain, lattice strain along different HKL planes (ε_{HKL}) are measured by comparing their d -spacing with theoretical values. On the other hand, ε_{HKL} is linearly dependent on the local elastic strain tensor ε_{ij} . Thus, the six unknown components of ε_{ij} can be determined by performing least square fitting if more than six HKL planes are used. The stress tensor can be further deduced from the elastic strain tensor by applying a general Hooke's law [57]. More recently, Oddershede et al.

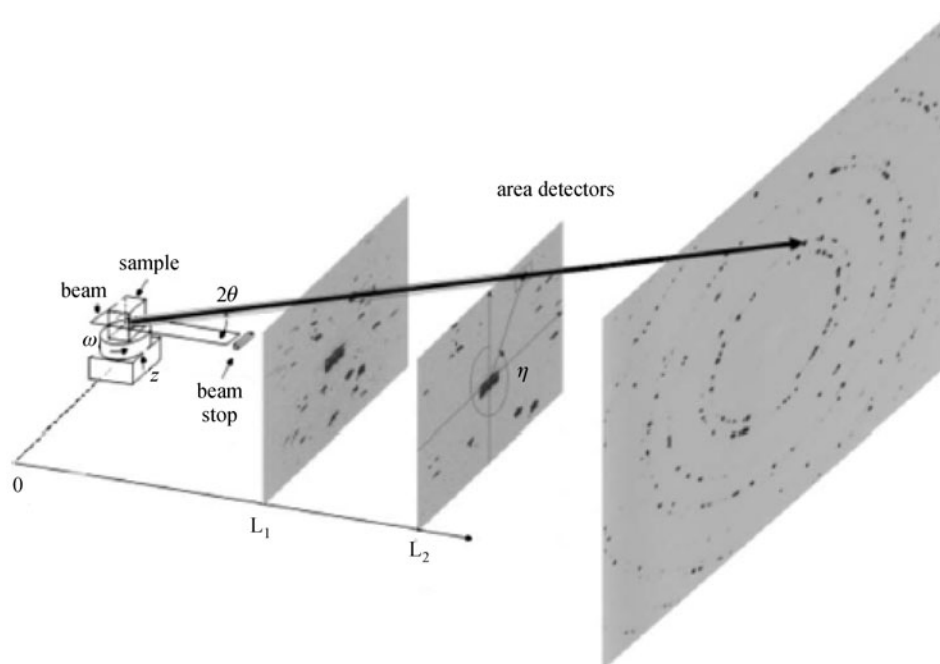


Fig. 4 3DXRD experimental setup. The incoming X-ray beam penetrates the specimen and generates diffraction patterns that are recorded by one or more 2D detectors. Diffraction spots on the near-field detector (closest to the specimen) are almost randomly distributed, while diffraction spots on the far-field detector form typical Debye–Scherrer rings. To obtain the complete microstructure, the specimen is rotated and an X-ray exposure is made for each rotation step. By taking all the recorded diffraction patterns together, the 3D grain structure and stress distribution in the illuminated material layer can be extracted. (Reproduced with permission from Ref. [48], <http://dx.doi.org/10.1107/S0021889812039143>, Copyright 2012 International Union of Crystallography)

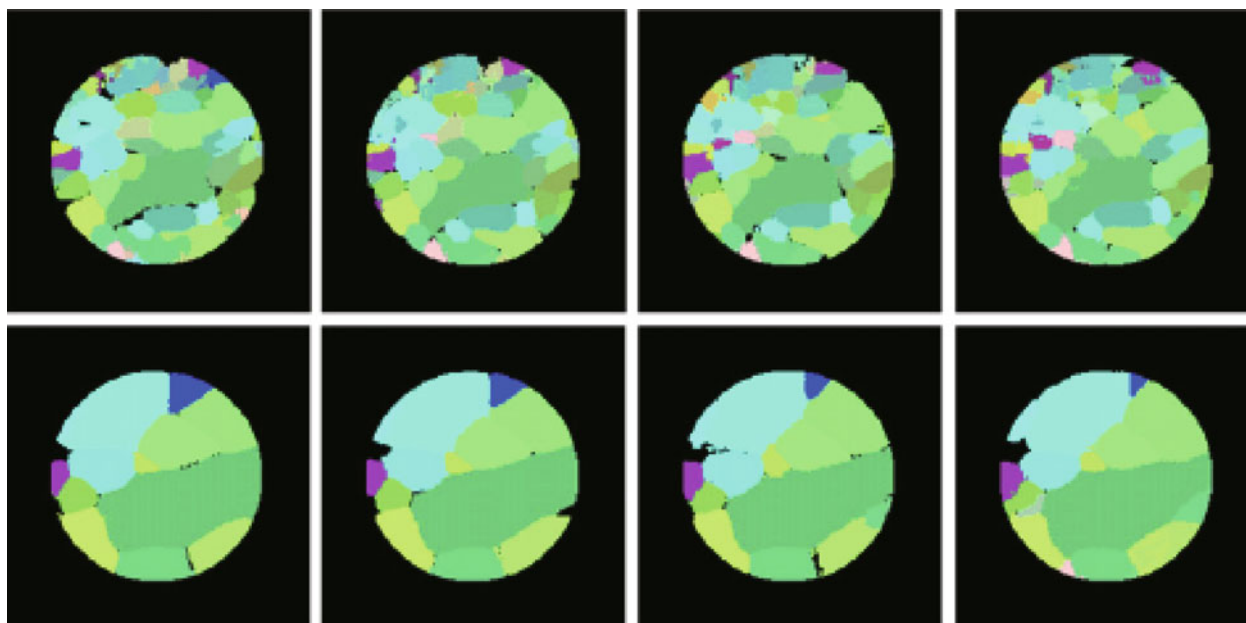


Fig. 5 Grain growth in Al-0.1%Mn revealed by 3DXRD using a near-field detector. Top row: grain maps of four layers in the material before annealing. Bottom row: corresponding grain maps of the same layers after annealing. The pixel size in the maps is $5\ \mu\text{m} \times 5\ \mu\text{m}$. (Reproduced with permission from Ref. [50], Copyright 2008 Acta Materialia Inc.)

[58–60] refine the fitting program to allow grain center position, grain orientation, and local elastic strain/stress tensor to be fitted altogether. Figure 6 shows the lattice rotation and stress distribution in a region that contains hundreds of grains in a deformed Mg alloy specimen [60].

Although 3DXRD is relatively new as a characterization tool and many technical details are still under development, it has already been used to investigate some fundamental problems in materials science. One example is the understanding of deformation twinning in hexagonal metals (e.g. Mg, Ti, Zr, etc.). For hexagonal metals, twinning is as important as dislocation slip for the material plasticity [61]. However, a convincing constitutive model that can accurately account for twin nucleation and subsequent growth is still under development [62–64]. (In contrast, dislocation slip can be well described by phenomenological or dislocation density based models [39,41,65].) Statistical analysis from EBSD characterization indicated that twin nucleation does not strictly follow the Schmid law, but depends on other factors such as parent grain size, grain boundary length, slip in the parent grain, and slip transfer from neighboring grains [66–69]. Unlike these *ex situ* surface observations, 3DXRD allows *in situ* observation of the formation of twins in the bulk material. Study of the strain/stress state in the parent grains can shed further light on the twin nucleation mechanism. Recently an *in situ* tensile test of a Ti polycrystalline specimen (cross section = $1\ \text{mm} \times 1\ \text{mm}$) at APS beamline 1-ID was performed to study twin nucleation behavior. The specimen was

incrementally deformed while being illuminated by a 70 keV beam (size = $700\ \mu\text{m} \times 250\ \mu\text{m}$). To include more grains, five consecutive layers of material along the gauge length were scanned by the beam for each load step. Diffraction patterns were processed by FABLE software package (<http://sourceforge.net/apps/trac/fable>) for peak searching, transformation, and grain identification. Grains were tracked based on their orientation and center position. After 1% strain, a few new grains were identified as twins along with their corresponding parent grains. Figure 7 shows one $\{10\bar{1}2\} \langle \bar{1}011 \rangle$ twin in the central layer as a new spot in the $\{0001\}$ pole figure after 1.5% strain. A parent grain that had the theoretical misorientation relationship with the twin was found in its vicinity. Using the method described in Ref. [52], the elastic strain tensor in the parent grain and the twin can be determined. Figure 7 shows the evolution of the normal component (e_{ZZ}), the transverse component (e_{YY}), and the associated shear component (e_{YZ}) of the elastic strain tensor in both the parent grain and the twin. In general, e_{ZZ} increased with global loading (along Z direction); e_{YY} decreased at a smaller slope; e_{YZ} was close to zero. Using the elastic strain tensor of the parent grain, the stress tensor and the resolved shear stress for the twinning system was calculated in order to evaluate the general Schmid law. Detailed results will be reported in a later paper.

To summarize, 3DXRD and DAXM are two complementary methods for probing microstructure in a bulk material. DAXM is best for probing near-surface fine

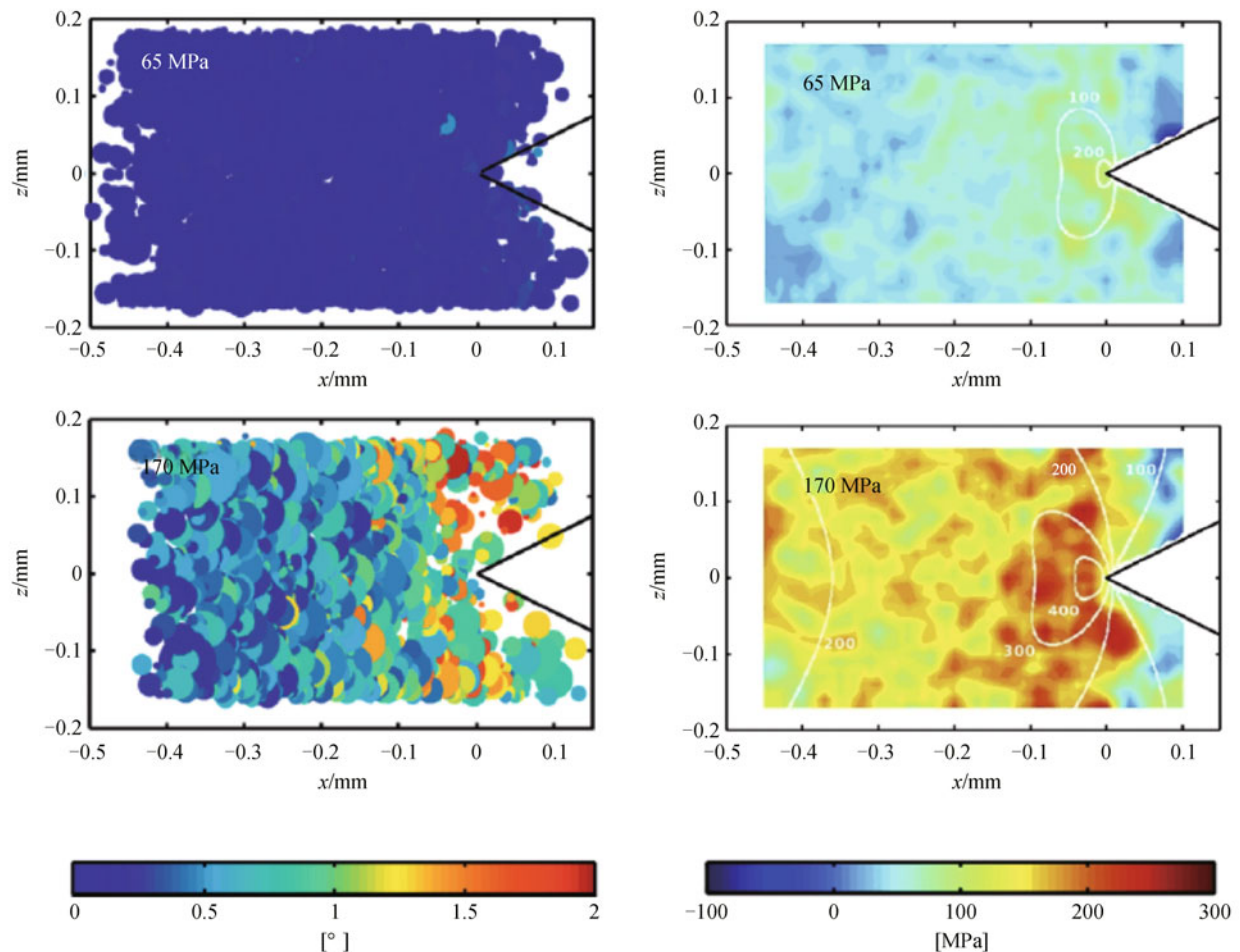


Fig. 6 Tensile deformation of an Mg alloy specimen with a notch. Left column: center of individual grains and the change in orientation at different applied stresses. The size of spheres represents the relative grain volume and the color code indicates the orientation change. Right column: distribution of the axial stress component in the same region. (Reproduced with permission from Ref. [60], Copyright 2012 Acta Materialia Inc.)

structure, with the advantage of a higher spatial resolution. 3DXRD is optimized for *in situ* bulk studies, with the advantage that a much larger volume can be assessed with higher energy X-rays.

4 Wide angle/small angle X-ray scattering

Grain-averaged X-ray diffraction (i.e. wide angle X-ray scattering, WAXS) is a widely used technique for phase identification and measuring texture, lattice parameter, and micro-strain. With the high penetration ability of synchrotron X-rays, *in situ* observation of microstructure evolution in bulk materials becomes possible. By conducting *in situ* tensile test using WAXS, Young et al. [70] studied the strengthening effect of Fe_3C precipitates in an ultrahigh-carbon steel (UHCS). In the elastic regime of this study, the Fe matrix and the Fe_3C precipitates developed the same amount of lattice strains. In the plastic regime, load transfer took place from the ductile α -Fe to the elastic Fe_3C , leading

to strain anisotropy in both phases. Similar results were reported by other authors for different alloys [71–73].

On the other hand, small angle X-ray scattering (SAXS) is often used for characterizing the average heterogeneous dispersion structure (e.g. precipitates/voids in metallic alloys, macromolecules in bio-systems, particles in gels, etc.) over the size range of ~ 1 –1000 nm. By fitting one-dimensional (1D) or 2D SAXS intensities versus d -spacing (or q -value), parameters such as size, shape, and distribution of the dispersed features/phases may be inferred [74].

Although WAXS and SAXS are historically performed individually using different detectors, simultaneous WAXS and SAXS can now be achieved by specialized detector configurations. Figure 8 demonstrates the scheme of simultaneous WAXS/SAXS at 1-ID beamline at APS. Four panels of WAXS 2D detectors are used, leaving an open space near the direct beam for a higher-resolution SAXS detector further downstream. Using simultaneous WAXS/SAXS, Pan et al. [75] correlated void formation

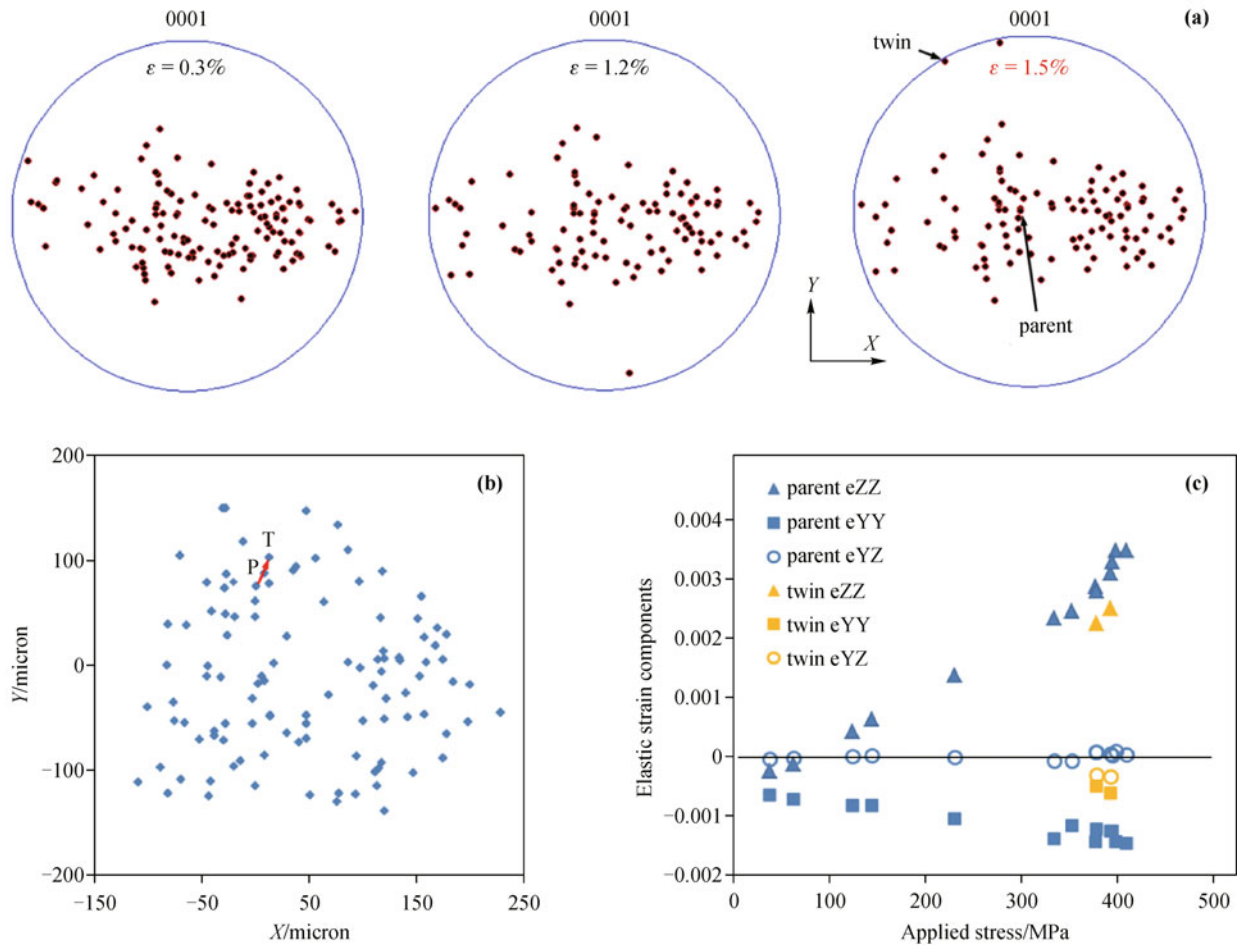


Fig. 7 *In situ* characterization of a twin and its parent grain in a Ti tensile specimen. **(a)** $\{0001\}$ pole figures at three different global strains. The normal direction is along the specimen loading direction Z. The twin spot appeared after 1.5% strain. Its parent grain was found based on misorientation and proximity to the twin in **(b)**, where the positions of all grains in a cross-section layer are plotted. The parent grain (P) and the twin (T) are noted. **(c)** The elastic strain evolution in the parent grain and the twin as a function of the applied stress.

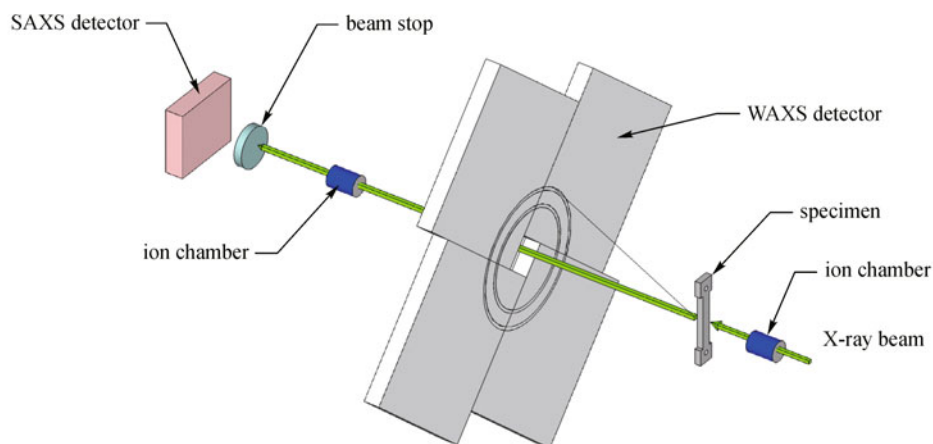


Fig. 8 Scheme for simultaneous WAXS/SAXS at 1-ID beamline at APS.

with matrix/precipitate lattice strain mismatch in order to elucidate the failure mechanism in precipitate-strengthened

steels while under thermo-mechanical loading. Figure 9 shows a recent result for *in situ* tensile tests of Grade 92

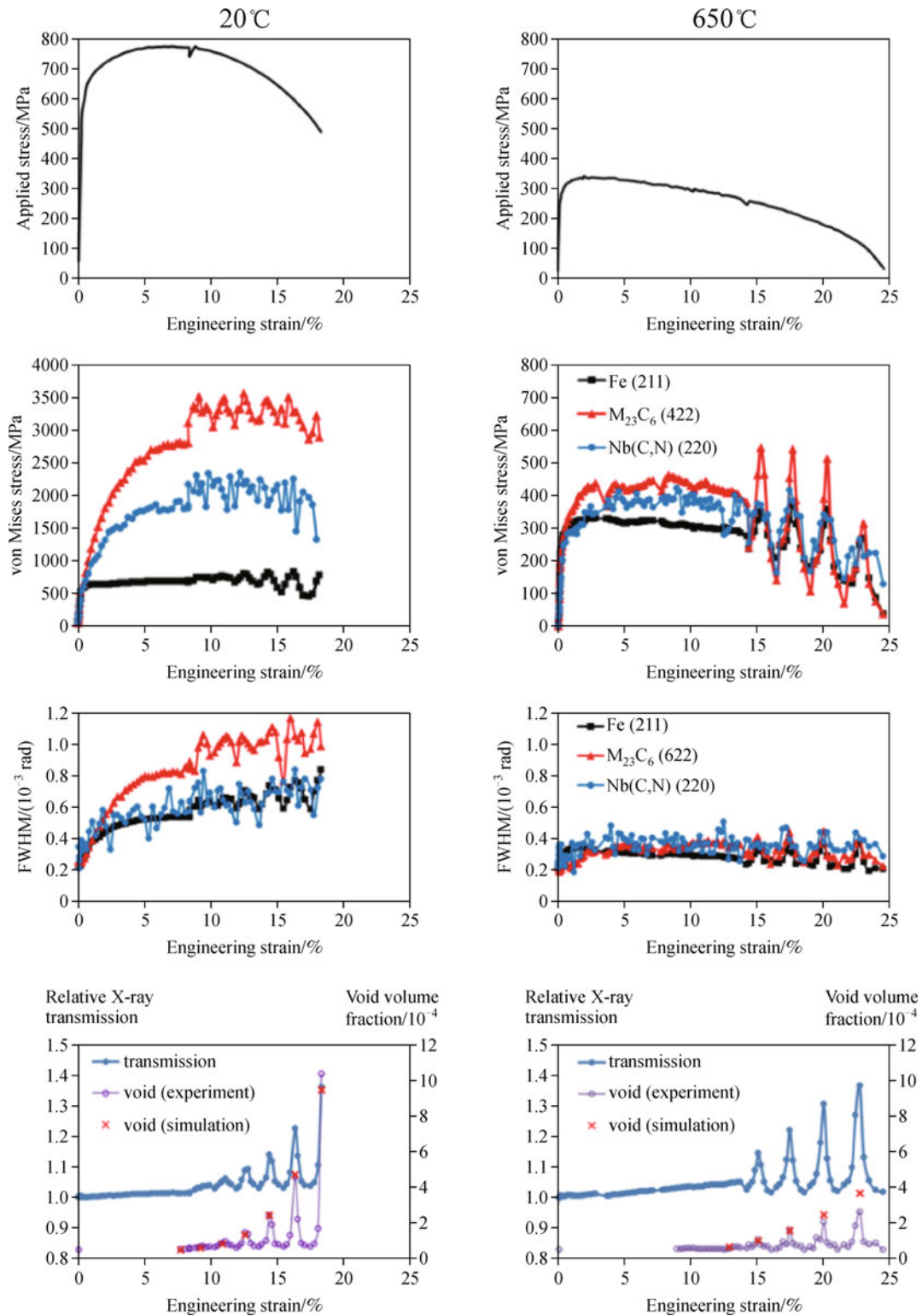


Fig. 9 *In situ* tensile tests of Grade 92 ferritic/martensitic steel at 20°C and 650°C by simultaneous WAXS/SAXS. Top row: macroscopic stress–strain curves showed a significant strength reduction from 20°C to 650°C. Second row: evolution of von Mises stress in Fe (black), $M_{23}C_6$ (red) and Nb(C,N) (blue) with strain. Third row: evolution of diffraction peak broadening in Fe (black), $M_{23}C_6$ (red) and Nb(C,N) (blue) with strain. Bottom row: volume fraction of voids as a function of strain was estimated from SAXS profiles. A strong correlation between void and necking (high X-ray transmission) was observed. The increase of void volume with strain at the necking center can be simulated by a mathematical model [76].

ferritic/martensitic steel (Fe–9Cr–1.8W–0.5Mo–0.2V–0.08Nb, wt.%). Specimens were deformed at a near constant strain rate of $1.3 \times 10^{-4} \text{ s}^{-1}$, while a 70 keV X-ray beam impinged on the specimens to generate WAXS and SAXS signals under different strains. In the uniform deformation stage (i.e. before necking), WAXS and SAXS patterns were continuously collected from the specimen's gauge center. After necking, the specimen was vertically scanned in the X-ray beam around the necking center (identified by the highest X-ray transmission point on the specimen) in order to evaluate non-uniform deformation. At 20°C, the material shows high yield strength. Evolution of the von Mises stress (deduced from lattice strain) indicates apparent load transfer from the Fe matrix to the $M_{23}C_6$ and Nb(C,N) precipitates after the onset of plastic deformation. Diffraction peak broadening increases with strain, which correlates to increased plastic deformation. According to SAXS intensity variations, voids started to form after necking and mostly concentrated at the necking center. At 650°C, the yield strength became much lower. Load transfer from matrix to precipitates as well as strain-induced peak broadening almost disappeared. The volume fraction of voids was lower than at 20°C at a similar extent of necking. The difference between 20°C and 650°C in terms of the stress–strain curve, load transfer, peak broadening, and void formation can be attributed to the different dislocation-precipitate interaction mechanisms at these two temperatures [76].

5 Summary and outlook

As a fundamental goal of materials science, microstructural characterization has been brought to a new level by the application of synchrotron X-rays. Three techniques, DAXM, 3DXRD, and WAXS/SAXS are described in this paper along with a few application examples.

Future development for DAXM will primarily focus on (i) making the beam size even smaller and (ii) making use of other signals from X-ray/material interaction. Over the last decade, it has been possible to reduce the beam size from 0.5 μm to 7 nm by improving X-ray optics [77]. Because almost all engineering materials are structurally inhomogeneous on multiple length scales, a smaller beam implies that finer structures in the material can now be characterized using X-ray diffraction (XRD). In addition to diffraction, X-rays generate other signals when interacting with the material, such as fluorescence and absorption spectroscopy. By installing proper detectors around the specimen, chemical composition, oxidation state, and local

coordination in the specimen can be extracted. There is potential for the current DAXM instrument to develop into a true nanoprobe for the study of materials with very fine structure.

With 3DXRD, improving the spatial resolution for 3D mapping is also vital. The primary strategy is to enhance resolution of the near-field detectors [48]. The codes for peak searching and grain indexing are being refined for application on multiphase materials. Also, combining 3DXRD with classical absorption or phase contrast tomography is being developed so that materials with complex structure can be better characterized.

WAXS/SAXS is ideal for characterizing heterogeneous structure in materials. This technique is particularly suitable for characterizing nuclear materials and fuels. Exposed to irradiation, a large population of defects such as voids, bubbles, dislocation loops are produced along with phase changes that can degrade the material performance [78]. High-energy X-rays offer an opportunity for *in situ* characterization of irradiated microstructure under thermal and mechanical loading, allowing direct correlation between microstructure and mechanical properties. Efforts are underway at the Argonne National Laboratory to develop such capability. Such efforts, if successful, will have a tremendous impact on the design and evaluation of new materials for future nuclear energy systems.

Abbreviations

1D	one-dimensional
2D	two-dimensional
3D	three-dimensional
3DXRD	three-dimensional X-ray diffraction
CPFEM	crystal plasticity finite element modeling
DAXM	differential-aperture X-ray microscopy
EBSDF	electron backscattering diffraction
EM	electron microscopy
FIB	focused ion beam
GND	geometrically necessary dislocation
HEDM	high energy diffraction microscopy
KB	Kirkpatrick-Baez
SAXS	small angle X-ray scattering
SEM	scanning electron microscopy
TEM	transmission electron microscopy
UHCS	ultrahigh-carbon steel
WAXS	wide angle X-ray scattering
XRD	X-ray diffraction

Acknowledgements The authors would like to thank Wenjun Liu, Martin Crimp, Carl Boehlert, Hongmei Li, Peter Kenesei, Ulrich Lienert, Armand Beaudoin, and Jan Ilavsky for their contribution to this paper. This work was

supported under the U.S. Department of Energy contract DE-AC02-06CH11357. R.B. is partially supported by US DOE office of science, basic energy science.

References

- [1] Hall E O. The deformation and ageing of mild steel: III Discussion of results. Proceedings of the Physical Society Section B, 1951, 64 (9): 747–753
- [2] Hertzberg R W. Deformation and Fracture Mechanics of Engineering Materials (4th Edition). New York: Wiley, 1996
- [3] Hull D, Bacon D J. Introduction to Dislocations. Oxford, UK: Elsevier, 2001
- [4] Kocks U F, Tome C N, Wenk H R. Texture and Anisotropy. Cambridge, UK: Cambridge University Press, 1998
- [5] Williams D B, Carter C B. Transmission Electron Microscopy. New York: Plenum Press, 1996
- [6] Goldstein J I, Newbury D E, Echlin P, et al. Scanning Electron Microscopy and X-Ray Microanalysis (3rd Edition). New York: Springer, 2003
- [7] Venables J A, Binjaya R. Accurate micro-crystallography using electron backscattering patterns. Philosophical Magazine, 1977, 35(5): 1317–1332
- [8] Dingley D J, Randle V. Microtexture determination by electron back-scatter diffraction. Journal of Materials Science, 1992, 27 (17): 4545–4566
- [9] Adams B L, Wright S I, Kunze K. Orientation imaging: The emergence of a new microscopy. Metallurgical Transactions A, 1993, 24(4): 819–831
- [10] Schwarz A J, Kumar M, Field D P, et al. Electron Backscatter Diffraction in Materials Science. New York: Springer, 2000
- [11] Bridier F, Villechaise P, Mendez J. Analysis of the different slip systems activated by tension in a α/β titanium alloy in relation with local crystallographic orientation. Acta Materialia, 2005, 53(3): 555–567
- [12] Bingert J F, Mason T A, Kaschner G C, et al. Deformation twinning in polycrystalline Zr: Insights from electron back-scattered diffraction characterization. Metallurgical and Materials Transactions A, 2002, 33(3): 955–963
- [13] Bieler T R, Eisenlohr P, Roters F, et al. The role of heterogeneous deformation on damage nucleation at grain boundaries in single phase metals. International Journal of Plasticity, 2009, 25(9): 1655–1683
- [14] Kral M V, Spanos G. Three-dimensional analysis of proeutectoid cementite precipitates. Acta Materialia, 1999, 47(2): 711–724
- [15] Zaefferer S, Wright S I, Raabe D. Three-dimensional orientation microscopy in a focused ion beam-scanning electron microscope: a new dimension of microstructure characterization. Metallurgical and Materials Transactions A, 2008, 39(2): 374–389
- [16] Uchic M D, Groeber M A, Rollett A D. Automated serial sectioning methods for rapid collection of 3-D microstructure data. JOM, 2011, 63(3): 25–29
- [17] Willmott P. An Introduction to Synchrotron Radiation: Techniques and Applications. New York: Wiley, 2011
- [18] Bilderback D H, Elleaume P, Weckert E. Review of third and next generation synchrotron light sources. Journal of Physics B: Atomic and Molecular Physics, 2005, 38(9): S773–S797
- [19] Larson B C, Yang W, Ice G E, et al. Three-dimensional X-ray structural microscopy with submicrometre resolution. Nature, 2002, 415(6874): 887–890
- [20] Ice G E, Barabash R I. White beam microdiffraction and dislocations gradients. Dislocations in Solids, Vol. 13, Chapter 79, 2007, 499–601
- [21] Liu W, Ice G E, Larson B C, et al. The three-dimensional X-ray crystal microscope: A new tool for materials characterization. Metallurgical and Materials Transactions A, 2004, 35(7): 1963–1967
- [22] Liu W, Ice G E, Larson B C, et al. Nondestructive three-dimensional characterization of grain boundaries by X-ray crystal microscopy. Ultramicroscopy, 2005, 103(3): 199–204
- [23] Wang L, Barabash R I, Yang Y, et al. Experimental characterization and crystal plasticity modeling of heterogeneous deformation in polycrystalline α -Ti. Metallurgical and Materials Transactions A, 2011, 42(3): 626–635
- [24] Larson B C, El-Azab A, Yang W, et al. Experimental characterization of the mesoscale dislocation density tensor. Philosophical Magazine, 2007, 87(8–9): 1327–1347
- [25] Barabash R I, Ice G E, Larson B C, et al. White microbeam diffraction from distorted crystals. Applied Physics Letters, 2001, 79(6): 749–751
- [26] Barabash R I, Ice G E, Walker F J. Quantitative microdiffraction from deformed crystals with unpaired dislocations and dislocation walls. Journal of Applied Physics, 2003, 93(3): 1457–1464
- [27] Barabash R I, Ice G E, Liu W, et al. Polychromatic microdiffraction characterization of defect gradients in severely deformed materials. Micron, 2009, 40(1): 28–36
- [28] Maass R, Van Petegem S, Van Swygenhoven H, et al. Time-resolved Laue diffraction of deforming micropillars. Physical Review Letters, 2007, 99(14): 145505 (4 pages)
- [29] Maaß R, Van Petegem S, Ma D, et al. Smaller is stronger: The effect of strain hardening. Acta Materialia, 2009, 57(20): 5996–6005
- [30] Kirchlechner C, Imrich P J, Grosinger W, et al. Expected and unexpected plastic behavior at the micron scale: An *in situ* μ Laue

- tensile study. *Acta Materialia*, 2012, 60(3): 1252–1258
- [31] Villechaise P, Sabatier L, Girard J C. On slip band features and crack initiation in fatigued 316L austenitic stainless steel: Part 1: Analysis by electron back-scattered diffraction and atomic force microscopy. *Materials Science and Engineering A*, 2002, 323(1–2): 377–385
- [32] Zaefferer S. A study of active deformation systems in titanium alloys: dependence on alloy composition and correlation with deformation texture. *Materials Science and Engineering A*, 2003, 344(1–2): 20–30
- [33] Li H, Boehlert C J, Bieler T R, et al. Analysis of slip activity and heterogeneous deformation in tension and tension-creep of Ti–5Al–2.5Sn (wt.%) using *in-situ* SEM experiments. *Philosophical Magazine*, 2012, 92(23): 2923–2946
- [34] Nye J F. Some geometrical relations in dislocated crystals. *Acta Metallurgica*, 1953, 1(2): 153–162
- [35] Arsenlis A, Parks D M. Crystallographic aspects of geometrically-necessary and statistically-stored dislocation density. *Acta Materialia*, 1999, 47(5): 1597–1611
- [36] Giannuzzi L A, Stevie F A. A review of focused ion beam milling techniques for TEM specimen preparation. *Micron*, 1999, 30(3): 197–204
- [37] Mayer J, Giannuzzi L A, Kamino T, et al. TEM sample preparation and FIB-induced damage. *MRS Bulletin*, 2007, 32(5): 400–407
- [38] Kalidindi S R, Bronkhorst C A, Anand L. Crystallographic texture evolution in bulk deformation processing of fcc metals. *Journal of the Mechanics and Physics of Solids*, 1992, 40(3): 537–569
- [39] Raabe D, Sachtleber M, Zhao Z, et al. Micromechanical and macromechanical effects in grain scale polycrystal plasticity experimentation and simulation. *Acta Materialia*, 2001, 49(17): 3433–3441
- [40] Musienko A, Tatschl A, Schmidegg K, et al. Three-dimensional finite element simulation of a polycrystalline copper specimen. *Acta Materialia*, 2007, 55(12): 4121–4136
- [41] Roters F, Eisenlohr P, Hantcherli L, et al. Overview of constitutive laws, kinematics, homogenization and multiscale methods in crystal plasticity finite-element modeling: Theory, experiments, applications. *Acta Materialia*, 2010, 58(4): 1152–1211
- [42] Poulsen H F, Garbe S, Lorentzen T, et al. Applications of high-energy synchrotron radiation for structural studies of polycrystalline materials. *Journal of Synchrotron Radiation*, 1997, 4(3): 147–154
- [43] Lauridsen E M, Schmidt S, Suter R M, et al. Tracking: a method for structural characterization of grains in powders or polycrystals. *Journal of Applied Crystallography*, 2001, 34(6): 744–750
- [44] Poulsen H F, Nielsen S F, Lauridsen E M, et al. Three-dimensional maps of grain boundaries and the stress state of individual grains in polycrystals and powders. *Journal of Applied Crystallography*, 2001, 34(6): 751–756
- [45] Margulies L, Winther G, Poulsen H F. *In situ* measurement of grain rotation during deformation of polycrystals. *Science*, 2001, 291(5512): 2392–2394
- [46] Poulsen H F. *Three-Dimensional X-ray Diffraction Microscopy*. Berlin: Springer, 2004
- [47] Lienert U, Li S F, Hefferan C M, et al. High-energy diffraction microscopy at the advanced photon source. *JOM*, 2011, 63(7): 70–77
- [48] Poulsen H F. An introduction to three-dimensional X-ray diffraction microscopy. *Journal of Applied Crystallography*, 2012, 45(6): 1084–1097
- [49] Suter R M, Hennessy D, Xiao C, et al. Forward modeling method for microstructure reconstruction using X-ray diffraction microscopy: Single-crystal verification. *Review of Scientific Instruments*, 2006, 77(12): 123905 (12 pages)
- [50] Schmidt S, Olsen U L, Poulsen H F, et al. Direct observation of 3-D grain growth in Al–0.1% Mn. *Scripta Materialia*, 2008, 59(5): 491–494
- [51] Li S F, Lind J, Hefferan C M, et al. Three-dimensional plastic response in polycrystalline copper via near-field high-energy X-ray diffraction microscopy. *Journal of Applied Crystallography*, 2012, 45(6): 1098–1108
- [52] Margulies L, Lorentzen T, Poulsen H F, et al. Strain tensor development in a single grain in the bulk of a polycrystal under loading. *Acta Materialia*, 2002, 50(7): 1771–1779
- [53] Martins R V, Margulies L, Schmidt S, et al. Simultaneous measurement of the strain tensor of 10 individual grains embedded in an Al tensile sample. *Materials Science and Engineering A*, 2004, 387–389: 84–88
- [54] Aydiner C C, Bernier J V, Clausen B, et al. Evolution of stress in individual grains and twins in a magnesium alloy aggregate. *Physical Review B*, 2009, 80(2): 024113 (6 pages)
- [55] Bernier J V, Barton N R, Lienert U, et al. Far-field high-energy diffraction microscopy: a tool for intergranular orientation and strain analysis. *Journal of Strain Analysis for Engineering Design*, 2011, 46(7): 527–547
- [56] Beaudoin A J, Obstalecki M, Storer R, et al. Validation of a crystal plasticity model using high energy diffraction microscopy. *Modelling and Simulation in Materials Science and Engineering*, 2012, 20(2): 024006 (14 pages)
- [57] Nye J F. *Physical Properties of Crystals: Their Representation by Tensors and Matrices*. New York: Oxford University Press, 1985
- [58] Oddershede J, Schmidt S, Poulsen H F, et al. Grain-resolved elastic strains in deformed copper measured by three-dimensional X-ray diffraction. *Materials Characterization*, 2011, 62(7): 651–660

- [59] Oddershede J, Schmidt S, Poulsen H F, et al. Determining grain resolved stresses in polycrystalline materials using three-dimensional X-ray diffraction. *Journal of Applied Crystallography*, 2010, 43(3): 539–549
- [60] Oddershede J, Camin B, Schmidt S, et al. Measuring the stress field around an evolving crack in tensile deformed Mg AZ31 using three-dimensional X-ray diffraction. *Acta Materialia*, 2012, 60(8): 3570–3580
- [61] Christian J W, Mahajan S. Deformation Twinning. *Progress in Materials Science*, 1995, 39(1–2): 1–157
- [62] Tome C N, Maudlin P J, Lebensohn R A, et al. Mechanical response of zirconium - I. Derivation of a polycrystal constitutive law and finite element analysis. *Acta Materialia*, 2001, 49(15): 3085–3096
- [63] Meyers M A, Vohringer O, Lubarda V A, et al. The onset of twinning in metals: A constitutive description. *Acta Materialia*, 2001, 49(19): 4025–4039
- [64] Beyerlein I J, Tome C N. A probabilistic twin nucleation model for HCP polycrystalline metals. *Proceedings of the Royal Society of London Series A*, 2010, 466(2121): 2517–2544
- [65] Ma A, Roters F, Raabe D, et al. A dislocation density based constitutive model for crystal plasticity FEM including geometrically necessary dislocations. *Acta Materialia*, 2006, 54(8): 2169–2179
- [66] Capolungo L, Marshall P E, McCabe R J, et al. Nucleation and growth of twins in Zr: A statistical study. *Acta Materialia*, 2009, 57(20): 6047–6056
- [67] Beyerlein I J, Capolungo L, Marshall P E, et al. Statistical analyses of deformation twinning in magnesium. *Philosophical Magazine*, 2010, 90(16): 2161–2190
- [68] Wang L, Yang Y, Eisenlohr P, et al. Twin nucleation by slip transfer across grain boundaries in commercial purity titanium. *Metallurgical and Materials Transactions A*, 2010, 41(2): 421–430
- [69] Wang L, Eisenlohr P, Yang Y, et al. Nucleation of paired twins at grain boundaries in titanium. *Scripta Materialia*, 2010, 63(8): 827–830
- [70] Young M L, Almer J D, Daymond M R, et al. Load partitioning between ferrite and cementite during elasto-plastic deformation of an ultrahigh-carbon steel. *Acta Materialia*, 2007, 55(6): 1999–2011
- [71] Cheng S, Wang Y D, Choo H, et al. An assessment of the contributing factors to the superior properties of a nanostructured steel using *in situ* high-energy X-ray diffraction. *Acta Materialia*, 2010, 58(7): 2419–2429
- [72] Colas K B, Motta A T, Almer J D, et al. *In situ* study of hydride precipitation kinetics and re-orientation in Zircaloy using synchrotron radiation. *Acta Materialia*, 2010, 58(20): 6575–6583
- [73] Weisser M A, Evans A D, Van Petegem S, et al. *In situ* room temperature tensile deformation of a 1% CrMoV bainitic steel using synchrotron and neutron diffraction. *Acta Materialia*, 2011, 59(11): 4448–4457
- [74] Guinier A, Fournet G. *Small-Angle Scattering of X-rays*. New York: Wiley, 1955
- [75] Pan X, Wu X, Mo K, et al. Lattice strain and damage evolution of 9–12%Cr ferritic/martensitic steel during *in situ* tensile test by X-ray diffraction and small angle scattering. *Journal of Nuclear Materials*, 2010, 407(1): 10–15
- [76] Wang L, Li M, Almer J D. *In situ* characterization of Grade 92 steel during tensile deformation using concurrent high energy X-ray diffraction and small angle X-ray scattering. *Journal of Nuclear Materials*, doi: 10.1016/j.jnucmat.2013.04.063 (in press)
- [77] Ice G E, Budai J D, Pang J W L. The race to X-ray microbeam and nanobeam science. *Science*, 2011, 334(6060): 1234–1239
- [78] Was G S. *Fundamentals of Radiation Materials Science*. Berlin: Springer, 2007